Journal of Inflammation Research

Dovepress
Taylor & Francis Group

Open Access Full Text Article

ORIGINAL RESEARCH

Single-Cell RNA Sequencing Reveals Pericytes Acquire a Fibrotic Phenotype and Promote Mesenteric Adipose Tissue Fibrosis in Crohn's Disease

Da Zhang[1,*], Anqi Yu[1,*], Mengjia He[1,*], Qian Zhou[1], Shibo Sun[2], Lan Bai[1], Fang Xie[1]

[1]Guangdong Provincial Key Laboratory of Gastroenterology, Institute of Gastroenterology of Guangdong Province, Department of Gastroenterology, Nanfang Hospital, Southern Medical University, Guangzhou, People's Republic of China; [2]Department of Hepatobiliary Surgery, Nanfang Hospital, Southern Medical University, Guangzhou, People's Republic of China

*These authors contributed equally to this work

Correspondence: Fang Xie, Guangdong Provincial Key Laboratory of Gastroenterology, Institute of Gastroenterology of Guangdong Province, Department of Gastroenterology, Nanfang Hospital, Southern Medical University, Guangzhou, 510515, People's Republic of China, Tel +86-020-61642511, Email stellaff@126.com

Purpose: Creeping fat (CF) in Crohn's disease (CD) is characterized by hyperplastic mesenteric adipose tissue (MAT) encasing fibrotic intestinal segments, marked by significant extracellular matrix (ECM) remodeling and fibrosis. Pericytes have multipotent differentiation potential, can adopt a fibrotic phenotype, and contribute to pathological ECM deposition. However, the cellular mechanisms underlying CF fibrosis remain unclear. This study aimed to elucidate the cellular origins of CF fibrosis and the involvement of pericytes.

Patients and Methods: Histopathological analyses evaluated fibrosis in MAT samples and its correlation with adjacent muscularis propria thickening. Transcriptomic datasets and immunofluorescence confirmed fibrosis-related gene expression differences in MAT. Single-cell RNA sequencing (scRNA-seq) was analyzed to evaluate ECM production across cell types and identify pericyte-specific markers. Cell proportion analyses and in vitro experiments quantified vascular endothelial and mural cell populations. CytoTRACE and pseudotime analyses mapped pericyte differentiation trajectories. Primary human MAT pericytes were isolated and stimulated with transforming growth factor-β1 (TGF-β1) to assess fibrotic phenotype transition in vitro.

Results: Fibrosis was evident in uninvolved MAT from CD patients (CD-MAT) and CF, with fibrosis severity in CF correlating positively with muscularis propria thickening. Core ECM gene COL3A1 was significantly upregulated in both CD-MAT and CF. CF exhibited increased endothelial and mural cell numbers. STEAP4 was identified as a pericyte-specific marker, with CF tissues showing higher pericyte abundance and enhanced perivascular ECM deposition. Pericytes in CD-MAT and CF adopted a fibrotic phenotype, marked by upregulation of COL3A1 and 18 other ECM genes. Furthermore, primary CD-MAT-derived pericytes treated with TGF-β1 displayed amplified fibrotic gene expression, confirming their profibrotic potential.

Conclusion: Pericytes in CF significantly expand and transition to a fibrotic phenotype, representing a key stromal cell population driving MAT fibrosis. These findings reveal an underrecognized cellular mechanism, highlighting novel therapeutic targets for MAT fibrosis.

Keywords: pericytes, creeping fat, fibrosis, Crohn's disease

Introduction

Crohn's disease (CD) is a chronic inflammatory disorder capable of affecting any segment of the gastrointestinal tract.[1,2] Over 50% of CD patients ultimately develop intestinal fibrosis and strictures, often necessitating surgical intervention.[3] Creeping fat (CF), a pathognomonic feature of CD, strongly correlates clinically and pathologically with transmural inflammation, muscular hypertrophy, fibrosis, and intestinal stricture formation.[4,5]

Received: 14 March 2025
Accepted: 8 August 2025
Published: 14 August 2025

Graphical Abstract

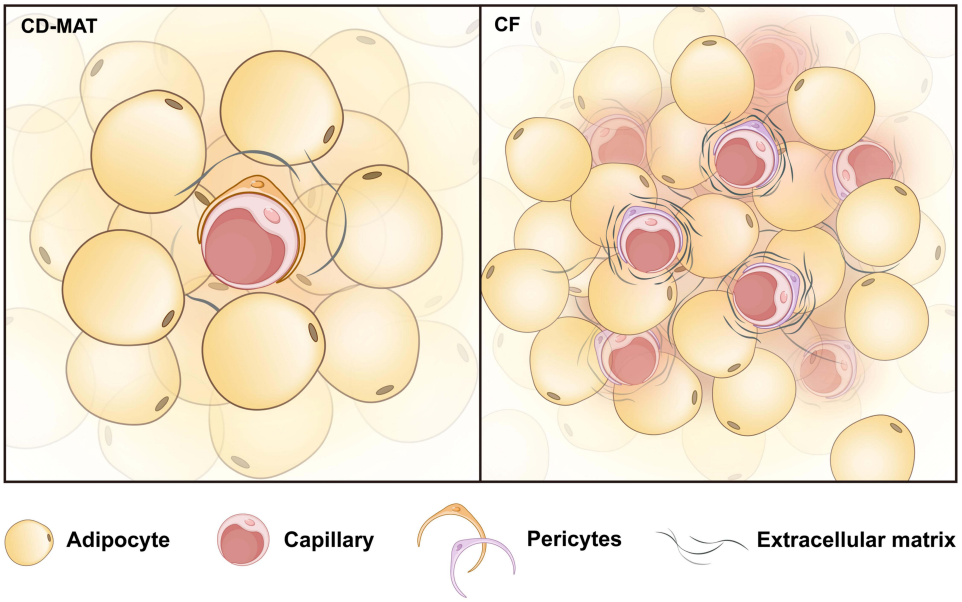

Under chronic inflammatory conditions, CF undergoes pathological remodeling characterized by extracellular matrix (ECM) deposition, immune cell infiltration, and impaired adipogenesis.[5,6] Notably, CF frequently coexists with intestinal strictures. Surgical specimens from CD patients exhibit extensive fibrosis penetrating mucosal layers, filling submucosal spaces, replacing muscularis propria in focal areas, and intercalating with mesenteric adipocytes.[7] More than 90% of ileal CD surgical samples display fibrosis within CF, primarily manifesting as fibrous bands traversing all tissue layers.[7] Samples with high fibrous band content show increased collagen turnover and elevated expression of key fibrotic genes compared to samples with low fibrous band content.[7] Scanning electron microscopy analyses have confirmed these findings, demonstrating disrupted adipocyte architecture, abnormal fiber networks, and ECM accumulation within CF.[6] Concurrent ECM synthesis and degradation in CF, indicated by the co-upregulation of matrix metalloproteinases (MMPs) and their inhibitors (TIMPs), highlight active ECM remodeling.[8] However, the precise mechanisms driving CF-related ECM remodeling and their impacts on mesenteric adipose tissue (MAT) and intestinal function remain poorly understood.[9]

Adipose tissue fibrosis is both a hallmark and a critical driver of adipose dysfunction, closely associated with metabolic disorders, cancer, atrial fibrillation, and osteoarthritis.[10–14] Pathological ECM remodeling in CF impairs mesenteric adipocyte function in CD.[8] Excessive ECM in CF acts as a reservoir for inflammatory cells and cytokines, such as tumor necrosis factor-α (TNF-α) and interleukin-6 (IL-6), which MMPs release via proteolytic cleavage, negatively impacting adipocyte function.[15,16] Furthermore, adipose fibrosis might influence fibrotic processes in adjacent organs, as subcutaneous adipose fibrosis correlates strongly with significant liver fibrosis,[17] and epicardial adipose fibrosis is linked to worsening myocardial fibrosis.[18] Importantly, gene expression patterns in high–fibrous-band CF samples correlate strongly with inflammatory fibroblast subsets in inflamed intestinal tissues of CD patients and can predict anti-TNF therapy responsiveness.[7,19] Clarifying MAT fibrosis mechanisms may yield novel diagnostic and therapeutic targets for CD.

Stromal vascular fraction (SVF) cells significantly contribute to ECM production in CF. Among these, mesenchymal stem cells (MSCs)—expressing platelet-derived growth factor receptor alpha (PDGFRA), decorin (DCN), and matrix metalloproteinase-2 (MMP2)—have been identified as primary ECM-producing cells.[6] However, tissue fibrosis involves diverse cell populations and complex mechanisms. Pericytes, vascular mural cells within the SVF expressing NOTCH3,[20] share multilineage differentiation capacity and fibrosis-associated gene expression with MSCs. Increasing evidence suggests pericytes transition

into fibrotic phenotypes and significantly contribute to fibrosis in organs like the kidney and heart.[21,22] Thus, pericytes may similarly promote MAT fibrosis in CF, though their specific role remains largely unexplored.

In this study, we collected human MAT samples and systematically analyzed the largest publicly available MAT transcriptomic dataset, alongside our previously published and independent single-cell RNA sequencing (scRNA-seq) datasets, to evaluate ECM deposition and fibrosis-related gene expression. Complementary in vitro experiments further aimed to define the contribution of pericytes to MAT fibrosis.

Materials and Methods

Ethics Approval and Consent to Participate

Patients were enrolled at Nanfang Hospital (Guangzhou, China) in compliance with the ethical principles of the Declaration of Helsinki. Ethical approval for this study was granted by the Medical Ethics Committee of Nanfang Hospital of Southern Medical University (approval number: NFEC-2024-495). Written informed consent was obtained from all participants prior to specimen collection and data acquisition. The diagnosis of CD was confirmed based on established criteria. Hyperplastic MAT adjacent to an inflamed, stenotic ileal segment was defined as CF, whereas uninvolved MAT from regions without active inflammation in CD patients was defined as CD-MAT. In addition, we collected histologically normal ileal MAT from grossly uninvolved regions of resected colorectal cancer specimens (confirmed to be free of tumor infiltration or inflammation). These samples served as a control group, referred to as H-MAT. Detailed demographic and clinical data for the enrolled CD patients are provided in Table S1.

Public Datasets Collection

We retrieved publicly available datasets from the Gene Expression Omnibus (GEO) database for both bulk transcriptomic and single-cell transcriptomic analyses of MAT. The GSE227376 dataset comprises bulk transcriptomic data from 59 individuals, including 23 paired CF and CD-MAT samples from CD patients and 13 H-MAT samples from non-CD individuals. The GSE215001 dataset provides single-cell transcriptomic data of MAT SVF cells from 6 CF samples, 3 CD-MAT samples, and 2 H-MAT samples. Lastly, the GSE156776 dataset includes single-cell transcriptomic data of MAT SVF cells from 2 CF and 2 H-MAT samples.

RNA-Seq Data Analysis

Differentially Expressed Gene (DEG) Analysis

We applied the DESeq2 algorithm to identify differentially expressed genes (DEGs) in bulk MAT transcriptomic data. Genes were considered differentially expressed if they met the following criteria after significance testing: (1) fold change > 2 or < 0.5, and (2) P-value < 0.05 with a false discovery rate (FDR) < 0.05. The R package ggplot2 (v3.4.1) was used to generate volcano plots and heatmaps of the DEGs.

scRNA-Seq Data Analysis

Quality Control of scRNA-Seq Data

Raw scRNA-seq reads were aligned to the human genome (GRCh38) using Cell Ranger (v7.1.0). Cells with fewer than 200 detected genes or more than 6000 detected genes, or with > 15% mitochondrial gene content, were filtered out as low quality. Ambient RNA contamination was removed using the SoupX package (v1.6.1), and potential doublets were identified and excluded using DoubletFinder (v2.0.3) with default parameters. Data quality control and normalization were performed with Seurat (v4.3.0).

Cell Clustering and Annotation

Normalized gene expression matrices were scaled to the total unique molecular identifier (UMI) count per cell and log-transformed. Highly variable genes (top 2000) were identified with Seurat's FindVariableFeatures, after which the data were centered and scaled. Principal component analysis (PCA) was performed using RunPCA, and batch effects were corrected with Harmony (RunHarmony). We constructed a k-nearest neighbor graph (k = 20) and performed clustering using FindNeighbors and FindClusters (resolution = 0.25). Clusters were visualized using Uniform Manifold Approximation and

Projection (UMAP; RunUMAP, dimensions 1–20). Cluster-specific marker genes were identified using FindAllMarkers (Wilcoxon rank-sum test, Bonferroni correction). Cell clusters were manually annotated based on known marker genes. The cellular composition of each sample was calculated as the proportion of each cell type, normalized to 100% for that sample.

DEG Analysis

Differential expression between cell subclusters was assessed using FindMarkers (Wilcoxon rank-sum test, Bonferroni correction). DEGs were defined as genes expressed in > 10% of cells in either group, with an absolute $\log_2$ fold change > 0.25 and adjusted P-value < 0.05.

Gene Ontology (GO) Enrichment Analysis

GO enrichment analysis was conducted using the clusterProfiler package (v3.14.3). Enrichment P-values were calculated via a hypergeometric test (significance threshold $P < 0.05$), and FDR was controlled using the Benjamini–Hochberg method. Bar plots were generated to visualize enriched pathways.

Trajectory Analysis

Cell trajectory analysis was performed with Monocle 2 (v2.14.0). Normalized counts were used to calculate pseudotime based on DEGs identified by Seurat's FindAllMarkers. Dimensionality reduction and cell ordering were performed using DDRTree and orderCells. DEGs along the pseudotime trajectory were identified using differentialGeneTest and visualized with plot_pseudotime_heatmap. Branch-specific DEGs were analyzed with BEAM and visualized with plot_genes_branched_heatmap (q-value < 1×10^{-4}).

CytoTRACE Analysis

VSMCs and pericytes were analyzed with CytoTRACE (v0.3.3) using default parameters. CytoTRACE differentiation scores were mapped onto the UMAP embedding for visualization.

Pathway Signature Module Score

Functional pathway signature scores for cell clusters were calculated using Seurat's AddModuleScore function. ECM-related pathway genes (collagens, glycoproteins, proteoglycans) were obtained from the MatrisomeDB 2.0 database. Data were visualized using ggplot2.

Isolation and Culture of Pericytes from Human MAT

Following established protocols, SVF cells were isolated from CD-MAT samples obtained during CD patient intestinal resections (see Table S1). The SVF cells were cultured and expanded in pericyte growth medium (ScienCell, Cat. 1201), a low-glucose medium supplemented with 2% fetal bovine serum (FBS), 1% penicillin–streptomycin, and 1% pericyte growth supplement. For magnetic-activated cell sorting (MACS), we used the EasySep™ system (STEMCELL Technologies). SVF cells were enzymatically dissociated with 2.5 g/L trypsin, resuspended at 1×10^7 cells/mL in phosphate-buffered saline (PBS) containing 2% FBS and 1 mM EDTA, and blocked with 1 μL EasySep™ Human CD32 FcR Blocker. We then added 3 μL of MCAM (CD146) monoclonal antibody (BioLegend, Cat. 361006) and incubated the cell suspension with the EasySep™ selection cocktail and RapidSpheres™ magnetic particles for 10 minutes. The suspension was placed in an EasySep magnet for 5 minutes, and the $MCAM^+$ cells that remained bound in the tube were collected. These cells were expanded in pericyte growth medium, and the sorting process was then repeated using a CD36 monoclonal antibody (BioLegend, Cat. 336203) to further enrich for pericytes.

TGF-β1 Stimulation

Purified pericytes were seeded at 8×10^4 cells per well in 6-well plates and cultured in pericyte growth medium for 2–3 days. The cells were then serum-starved in 0.2% FBS pericyte medium for 8 hours before stimulation with 10 ng/mL transforming growth factor-β1 (TGF-β1; Novoprotein, Cat. CA59). After 24 hours of stimulation, gene expression changes were assessed by quantitative reverse transcription PCR.

Immunofluorescence

Paraffin-embedded intestinal tissue sections (5 μm thick) were deparaffinized in xylene and rehydrated through a graded ethanol series. Antigen retrieval was performed by heating the sections in 10 mM citrate buffer (pH 6.0) at 100 °C. Endogenous peroxidase activity was quenched with 3% hydrogen peroxide, followed by blocking with normal serum. Sections were incubated overnight at 4 °C with primary antibodies against CD31 (1:200, rabbit monoclonal, Servicebio, Cat. GB11063-2), MCAM (CD146; 1:1000, rabbit monoclonal, Abcam, Cat. ab75769), α-SMA (α–smooth muscle actin; 1:200, rabbit monoclonal, Cell Signaling Technology, Cat. 19245), COL3A1 (1:1000, rabbit monoclonal, Abcam, Cat. ab7778), and STEAP4 (1:100, rabbit monoclonal, Proteintech, Cat. 11944-1-AP). After washing, sections were incubated with secondary antibodies (Alexa Fluor 488–conjugated donkey anti-rabbit IgG (H+L) and Alexa Fluor 594–conjugated donkey anti-rabbit IgG (H+L); both 1:400, Abcam, Cat. ab150073 and ab150076). Stained sections were examined using an Olympus BX-53 microscope.

For cultured cells, pericytes were grown on glass coverslips in 24-well plates and fixed with 4% paraformaldehyde at ~50% confluency. Cells were permeabilized with 0.2% Triton X-100, blocked with 5% bovine serum albumin (BSA), and incubated overnight at 4 °C with primary antibodies against STEAP4 (1:100, rabbit monoclonal, Proteintech, Cat. 11944-1-AP), MCAM (1:1000, rabbit monoclonal, Abcam, Cat. ab75769), α-SMA (1:200, rabbit monoclonal, Cell Signaling Technology, Cat. 19245), and COL3A1 (1:1000, rabbit monoclonal, Abcam, Cat. ab7778). After washing, cells were incubated with Alexa Fluor 488–conjugated donkey anti-rabbit IgG (H+L) secondary antibodies (1:400). The slides were then examined with an Olympus BX-53 microscope.

Gene Expression Analysis by Quantitative Reverse Transcription PCR

Total RNA was extracted using TRIzol reagent (Takara) according to the manufacturer's instructions. First-strand cDNA was synthesized using PrimeScript™ RT Master Mix (Takara). Quantitative PCR (qPCR) was performed using SYBR Green Master Mix (Takara) on a LightCycler 480 system (Roche). mRNA levels of target genes were calculated using the $2^{-\Delta\Delta CT}$ method and normalized to PPIA (cyclophilin A). Primer sequences are listed in Table S2.

Statistics and Reproducibility

Statistical analyses were performed using GraphPad Prism 8.0 (GraphPad Software) and R. Differences between two groups were assessed with the Student's *t*-test or the Mann–Whitney *U*-test. Comparisons among three groups were performed using the Kruskal–Wallis test. Details of specific statistical tests are provided in the figure legends. A P-value < 0.05 was considered statistically significant. Significance levels are indicated as *P < 0.05, **P < 0.01, ***P < 0.001, and ****P < 0.0001.

Results

ECM Deposition and Fibrosis-Related Gene Expression in MAT

Previous studies of MAT fibrosis have primarily focused on CF.[6,7] Our scanning electron microscopy analysis demonstrated increased ECM deposition in a CD-MAT sample,[6] suggesting the presence of fibrosis and dysfunction in CD-MAT. To further validate fibrosis in CD-MAT, we collected 83 human MAT samples (15 H-MAT, 34 CD-MAT, and 34 CF). Clinical data for the tissues used in histopathological analysis are provided in Table S1. Masson's trichrome staining of H-MAT, CD-MAT, and CF samples revealed no excessive ECM deposition in H-MAT (Figure 1A and B). In CD-MAT, ECM deposition was increased compared to H-MAT; however, fibrous bands characteristic of penetrating fibrosis (as seen in CF) were not present.[7] Notably, a significant portion of the ECM in CD-MAT was deposited around blood vessels (Figure 1A and B). In contrast, CF demonstrated a pronounced increase in ECM deposition relative to both H-MAT and CD-MAT, characterized by fibrous bands partitioning the adipose tissue, smaller adipocytes, and ECM accumulation within interstitial spaces (Figure 1A and B). To quantify differences in collagen deposition, we measured the collagen volume fraction (CVF) in Masson's trichrome–stained sections. We observed a stepwise increase in CVF from H-MAT to CF. Both CD-MAT and CF had significantly higher CVF than H-MAT, confirming excessive ECM deposition (Figure 1C). In areas of more severe fibrosis, we also noted pronounced thickening of the adjacent muscularis propria. Indeed, CVF was positively correlated with muscularis propria thickness in stenotic intestinal segments in CD (Figure 1D).

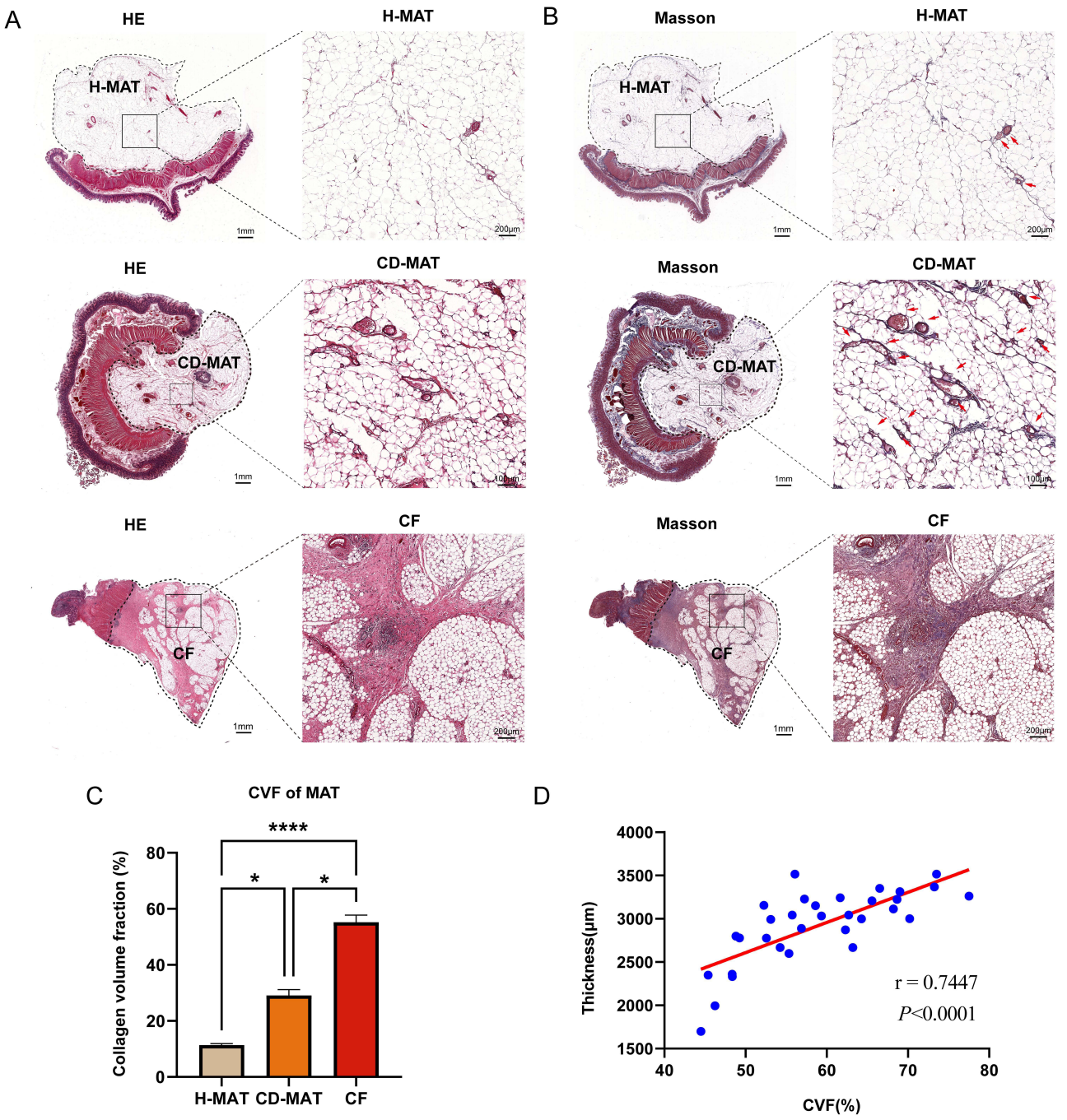

Figure 1 Histological evaluation of the three mesenteric adipose tissue (MAT) groups (H-MAT, CD-MAT, and CF). (**A** and **B**) Representative images of MAT sections from H-MAT, CD-MAT, and CF groups stained with hematoxylin and eosin (H&E) (**A**) and Masson's trichrome (**B**). In panel B, red arrows indicate the location and distribution of blood vessels and surrounding collagen in H-MAT and CD-MAT tissues. (**C**) Quantitative analysis of collagen volume fraction (CVF) based on Masson's trichrome staining in the three groups. Data are presented as mean ± SEM. Statistical significance: **P* < 0.05, *****P* < 0.0001 (Kruskal–Wallis test with adjusted *P*-values). (**D**) Spearman correlation between mesenteric adipose tissue CVF and muscularis propria thickness in intestinal tissues from CD patients.

To systematically evaluate fibrosis-related gene expression differences across the three groups, we compiled a set of 171 core ECM-related genes involved in collagen, glycoprotein, and proteoglycan biosynthesis (see Table S3).[23] We then performed a comprehensive analysis using publicly available transcriptomic data from 23 paired CF and CD-MAT samples and 13 H-MAT samples.[24] Heatmap analysis of core ECM gene expression showed an overall upregulation in both CD-MAT and CF compared to H-MAT (Figure 2A). Differential gene expression analysis revealed the greatest number of DEGs in CF versus H-MAT (627 upregulated, 238 downregulated), followed by CF versus CD-MAT (329 upregulated, 35 downregulated),

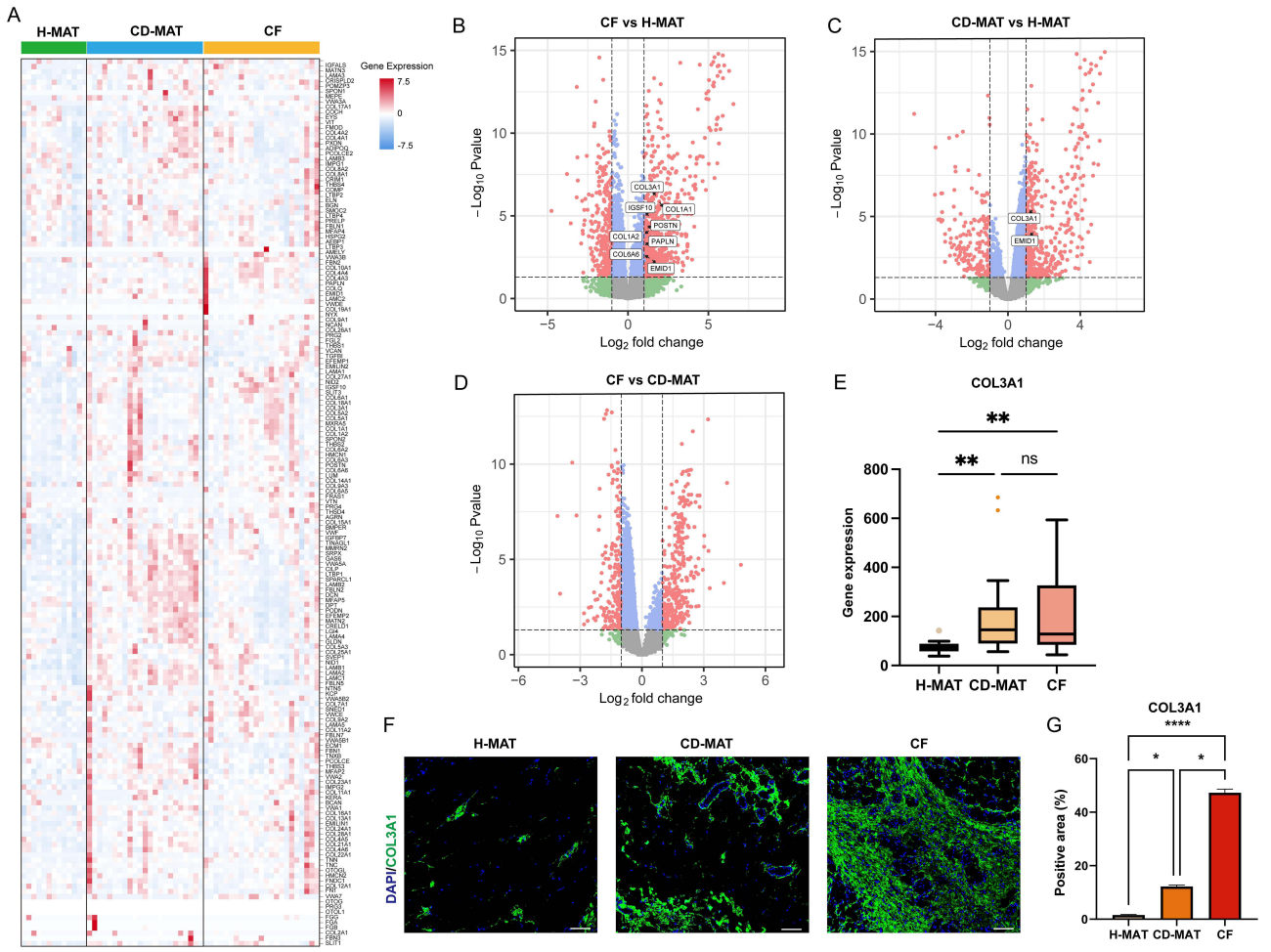

Figure 2 Differential gene expression analysis in the three MAT groups. (**A**) Heatmap showing the expression patterns of 171 core ECM genes across H-MAT, CD-MAT, and CF samples. (**B–D**) Volcano plots illustrating differentially expressed genes (DEGs) between (**B**) CF and H-MAT, (**C**) CD-MAT and H-MAT, and (**D**) CF and CD-MAT. (**E**) Box plot comparing COL3A1 gene expression among H-MAT, CD-MAT, and CF samples. The central line indicates the median, and the box hinges correspond to the first and third quartiles. Statistical significance: $^{**}P < 0.01$ (Kruskal–Wallis test with adjusted *P*-values). (**F**) Representative immunofluorescence images showing COL3A1 (green) with nuclear counterstain DAPI (blue) in the three MAT groups. Scale bars: 100 μm. (**G**) Quantification of COL3A1 fluorescence intensity, indicating significantly higher expression in CD-MAT and CF compared to H-MAT. Data are mean ± SEM. Statistical significance: $^{*}P < 0.05$, $^{****}P < 0.0001$ (Kruskal–Wallis test with adjusted *P*-values).

and the fewest in CD-MAT versus H-MAT (208 upregulated, 140 downregulated). Eight core ECM genes (COL1A1, COL1A2, COL3A1, COL6A6, POSTN, EMID1, IGSF10, PAPLN) were significantly upregulated in CF versus H-MAT (Figures 2B and S1), while COL3A1 and EMID1 were the only core ECM genes significantly upregulated in CD-MAT versus H-MAT (Figures 2C and S1). Notably, none of the core ECM genes were differentially expressed between CD-MAT and CF (Figure 2D). COL3A1 emerged as the only core collagen gene concurrently upregulated in both CD-MAT and CF cohorts (Figure 2E). Immunofluorescence staining confirmed higher COL3A1 protein expression in both CD-MAT and CF compared to H-MAT (Figure 2F and G). In summary, while CF exhibits the most severe overall fibrosis, overall MAT fibrosis is not limited to CF and is present to a lesser extent in CD-MAT.

MSCs and Mural Cells as Key ECM Producers in Human MAT

To identify the SVF subpopulations that contribute to MAT fibrosis, we analyzed two scRNA-seq datasets of MAT SVF cells. The primary dataset included 6 CF, 3 CD-MAT, and 2 H-MAT samples,[6] while the validation dataset comprised 2 CF and 2 H-MAT samples.[4] After stringent quality control, we obtained 60,168 high-quality cells in the primary dataset and 8750 in the validation dataset. Unsupervised clustering identified 13 distinct SVF cell subpopulations in the primary dataset (Figure 3A): T cells 1 (CCL5, GZMK, CCL4), T cells 2 (IL7R, TRBC2, CD2), NK cells (GNLY, NKG7, GZMB),

https://doi.org/10.2147/JIR.S528171

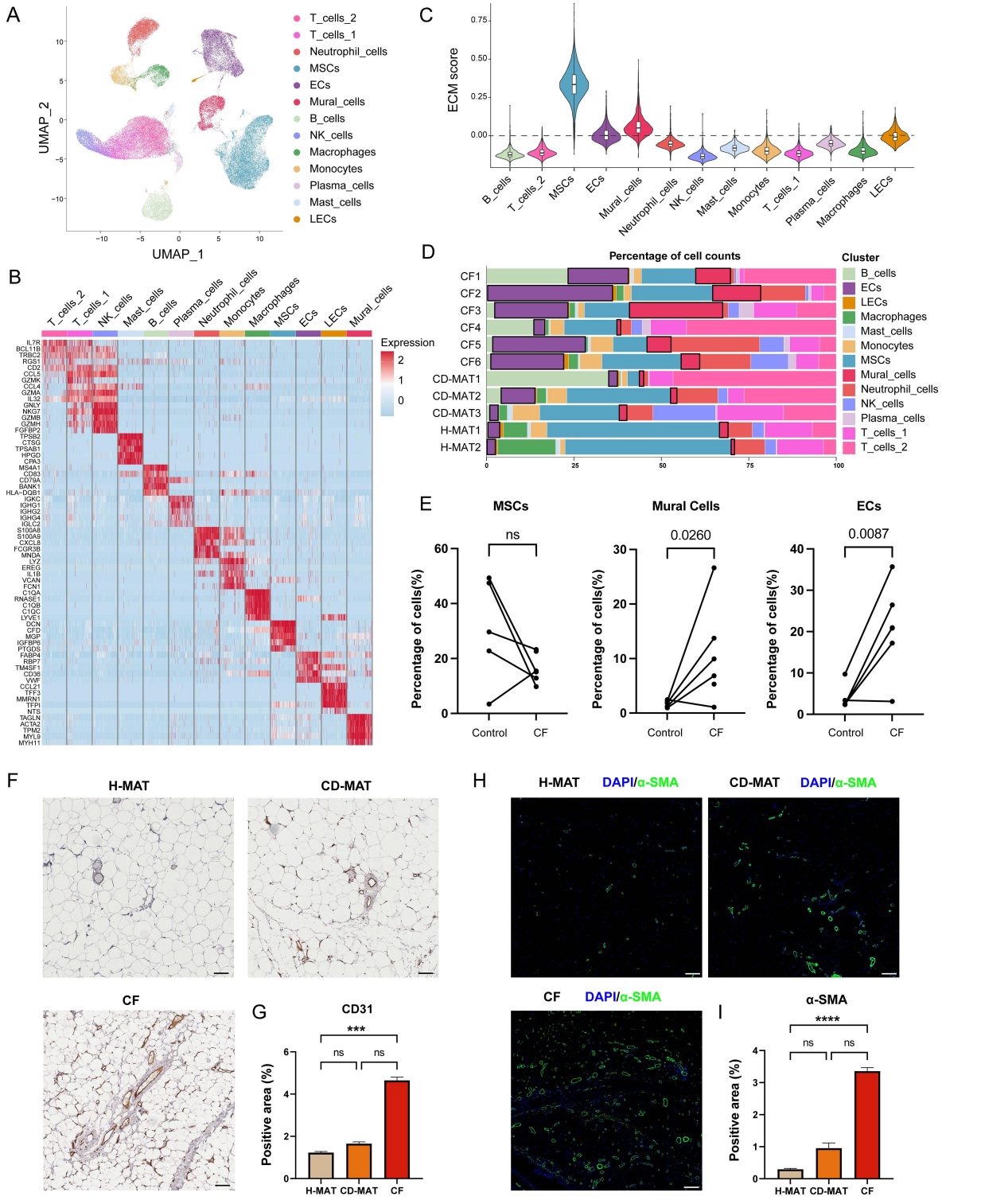

Figure 3 Subclustering and ECM scoring of stromal vascular fraction (SVF) cells in human MAT. (**A**) UMAP plots of scRNA-seq data showing thirteen distinct cell clusters across H-MAT, CD-MAT, and CF tissues. (**B**) Heatmap depicting scaled expression of representative marker genes for each of the thirteen clusters. (**C**) Violin plots of ECM scores for each cell cluster. (**D**) Stacked bar plots showing the relative proportions of each cell type within the SVF of each group. (**E**) Comparison of the proportions of MSCs, mural cells, and endothelial cells (ECs) between the control group (combined H-MAT and CD-MAT, n = 5) and the CF group (n = 6). Statistical significance was determined by the Mann–Whitney *U*-test with adjusted *P*-values. (**F**) Representative immunohistochemical staining for CD31 in MAT sections from the three groups. Scale bars: 100 μm. (**G**) Quantification of endothelial cell density, showing an increase in CF tissues compared to combined H-MAT/CD-MAT controls. Data are mean ± SEM. Statistical significance: ***$P < 0.001$ (Kruskal–Wallis test with adjusted *P*-values). (**H**) Representative immunofluorescence staining of α-SMA (green) in MAT sections from each group. Scale bars: 100 μm. (**I**) Quantitative analysis showing increased mural cell density in CF compared to combined H-MAT/CD-MAT controls. Data are mean ± SEM. Statistical significance: ****$P < 0.0001$ (Kruskal–Wallis test with adjusted *P*-values).

mast cells (CPA3, TPSB2, CTSG), B cells (MS4A1, CD83, CD79A), plasma cells (IGKC, IGHG1, IGHG2), neutrophils (S100A8, S100A9, CXCL8), monocytes (LYZ, EREG, IL1B), macrophages (C1QA, C1QB, C1QC), MSCs (DCN, CFD, MGP), endothelial cells (ECs; FABP4, CD36, VWF), lymphatic ECs (LECs; CCL21, TFF3, NTS), and mural cells (TAGLN, ACTA2, MYH11) (Figure 3B). In the validation dataset, 9 similar SVF subpopulations were identified: T cells, NK cells, B cells, plasma cells, neutrophils, macrophages, MSCs, ECs, and mural cells (Figure S2A and B).

We then assessed the ECM production capacity of each SVF subpopulation by calculating an ECM score based on the 171 core ECM-related genes. Among all SVF subpopulations, only MSCs and mural cells exhibited ECM scores consistently above zero, indicating a higher overall ECM-producing capacity (Figure 3C). The relative distribution of ECM scores among SVF subpopulations was consistently reproduced in the validation dataset, reinforcing the conclusion that MSCs and mural cells are the predominant ECM-producing cells in MAT (Figure S2C).

Cellular composition analysis revealed significant differences between CF tissues and control tissues (the control group comprised combined H-MAT and CD-MAT samples). Specifically, CF samples had markedly higher proportions of mural cells and ECs compared to the control group (Figure 3D and E). Immunohistochemical staining for CD31 (an EC marker) confirmed a significant increase in endothelial cells in CF compared to both H-MAT and CD-MAT (Figure 3F and G). α–Smooth muscle actin (α-SMA), expressed by MAT mural cells (see Figure 3B), served as a marker for these cells. Immunofluorescence staining for α-SMA revealed a significant increase in mural cells in CF compared to H-MAT and CD-MAT (Figure 3H and I). Together, these results indicate that CF tissue displays a significantly increased vascular density relative to H-MAT and CD-MAT.

As the primary ECM-producing population in MAT, MSCs were further examined for their fibrogenic potential. The proportion of MSCs did not differ significantly between CF and control tissues (Figure 3D and E). To gain deeper insight, we performed subclustering of the MSC population and assessed ECM production in each subcluster. Based on gene expression patterns, we identified three MSC subclusters: MSC1 (FBN1, SEMA3C, CD55), MSC2 (SFRP4, DDIT4, ADIRF), and MSC3 (APOE, CXCL14, C7) (Figure S3A and B). ECM score analysis showed that all three MSC subclusters had comparable fibrogenic capacities (Figure S3C and D), suggesting that these MSC subpopulations have similar potential to promote MAT fibrosis.

Mural Cell Subpopulations in MAT Fibrosis

Mural cells, which include vascular smooth muscle cells (VSMCs) and pericytes, surround blood vessels on the abluminal side adjacent to ECs.[25,26] While the roles of these cells in vascular biology are well established, their contribution to MAT fibrosis is poorly understood. To investigate this, we subdivided the mural cell population in both the primary and validation datasets. We found that mural cells segregated into two groups corresponding to VSMCs and pericytes (Figures 4A and S4A). Gene Ontology pathway analysis revealed that VSMCs were enriched in pathways related to muscle contraction and oxidative phosphorylation, whereas pericytes were enriched in pathways related to ECM organization, wound healing, cell adhesion, and regulation of endothelial cells (Figures 4B and S4B).

Heatmap analysis of DEGs showed that VSMCs highly expressed smooth muscle genes (MYH11, DSTN, CNN1, ACTG2, DES), whereas pericytes had elevated expression of ECM-related genes (COL1A1, COL1A2, COL3A1, THY1, POSTN) (Figures 4C and S4C). Both subpopulations shared canonical mural cell markers (MCAM, ACTA2, NOTCH3, PDGFRB) (Figures 4D and S4D). Notably, RERGL was uniquely expressed in VSMCs, whereas STEAP4 was uniquely expressed in pericytes (Figures 4D and S4D). These findings were further supported by histology: H&E staining and immunofluorescence co-staining in CF tissue confirmed that STEAP4 was highly expressed in pericytes but only weakly (or not at all) in VSMCs, while MCAM and α-SMA were expressed in both cell types (Figure 4E).

Differentiation Pathways of Pericytes in MAT

To compare the ECM-producing capacity of VSMCs and pericytes under different disease conditions, we calculated ECM scores for each subpopulation across H-MAT, CD-MAT, and CF samples. In all three groups, pericytes consistently exhibited higher ECM scores than VSMCs (Figure 5A). Moreover, both cell types showed a progressive increase in ECM scores from H-MAT to CD-MAT to CF (Figure 5A). These results indicate that the fibrotic phenotype of pericytes becomes progressively more pronounced with disease severity, particularly in CF. To further explore whether pericytes

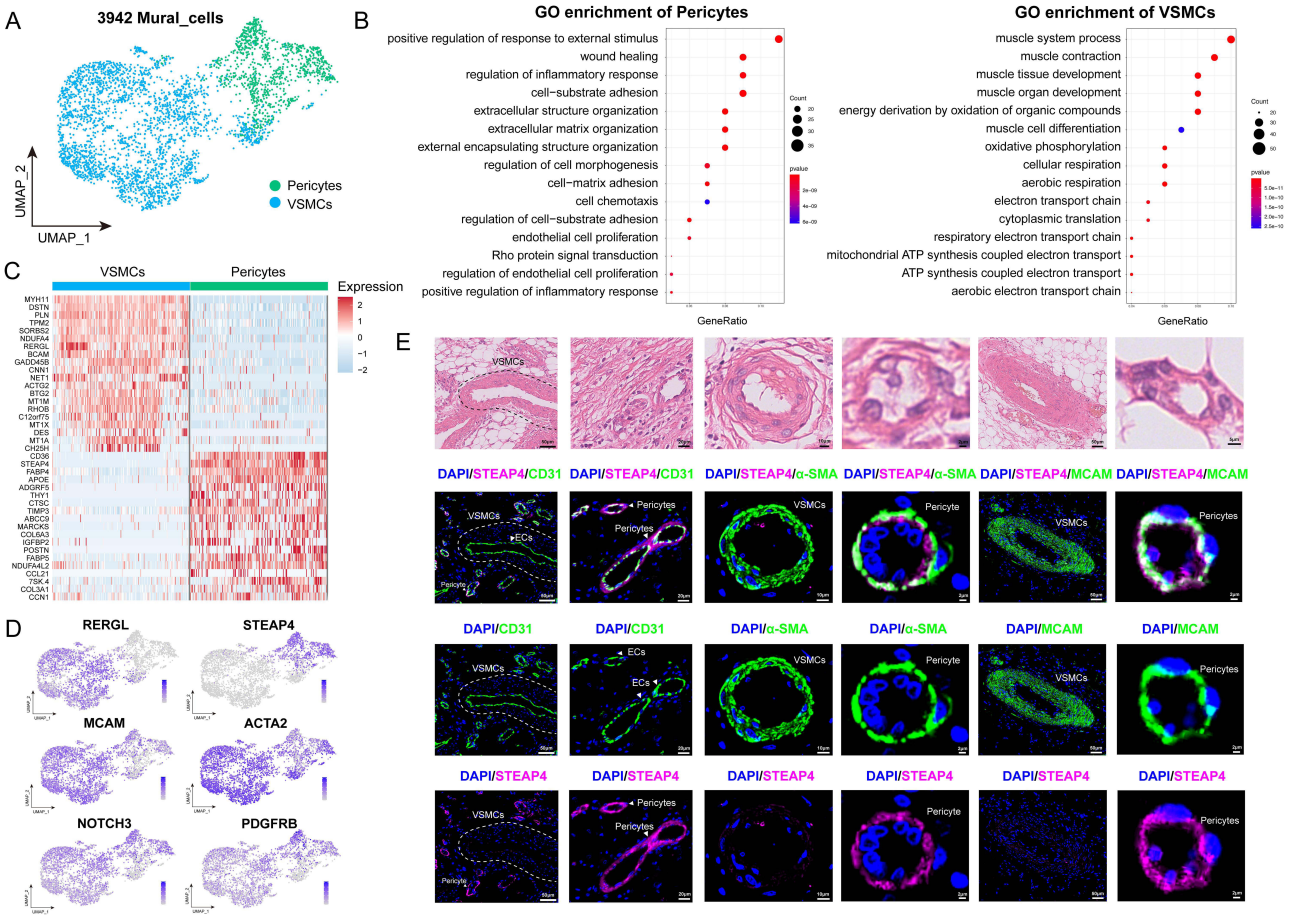

Figure 4 Vascular mural cells in human MAT can be subdivided into pericytes and vascular smooth muscle cells (VSMCs). (**A**) UMAP plot of mural cells showing two distinct subsets: pericytes and VSMCs. (**B**) Dot plot of enriched GO terms in pericytes versus VSMCs (bubble size represents the number of genes; color intensity indicates −log [*P*-value]). (**C**) Heatmap illustrating expression levels of marker genes distinguishing VSMCs from pericytes (red = high expression, blue = low). (**D**) UMAP feature plots showing expression of selected marker genes specific to VSMCs and pericytes. (**E**) Representative histological and immunofluorescence images of human MAT, including H&E staining and immunostaining for CD31 (green), STEAP4 (magenta), α-SMA (green), and MCAM (green), with nuclear counterstain DAPI (blue).

undergo a fibrotic phenotypic switch, we evaluated the differentiation potential of both subpopulations using CytoTRACE,[27] an algorithm that infers relative differentiation state. This analysis showed that pericytes have a significantly higher differentiation potential than VSMCs (Figure 5B).

Trajectory analysis using Monocle 2 revealed that pericytes can differentiate along two distinct paths, designated Fate 1 and Fate 2 (Figure 5C). Gene expression heatmaps showed that during the transition from the pre-state to Fate 1, 19 core ECM genes were upregulated, indicating a shift toward a fibrotic phenotype. Conversely, the transition from the pre-state to Fate 2 involved upregulation of VSMC-specific markers (RERGL, NTRK2, MYL9, DSTN, ACTA2), indicating differentiation of pericytes into VSMCs (Figure 5D).

Further analysis of the pseudotime trajectories revealed that pericyte differentiation into a fibrotic phenotype occurred predominantly in CF and CD-MAT, and was not observed in H-MAT. In both CF and CD-MAT, pre-state pericytes differentiated toward Fate 1, accompanied by a marked increase in expression of the core ECM gene COL3A1 (Figure 5E). This fibrotic transition of pericytes may partly account for the elevated COL3A1 expression observed at the tissue level in CD-MAT and CF (Figure 2F and G). In contrast, differentiation of pericytes into VSMCs occurred mainly in CF and H-MAT, and was not seen in CD-MAT. In those cases, pre-state pericytes transitioned toward Fate 2, characterized by increased expression of the VSMC marker RERGL (Figure 5E).

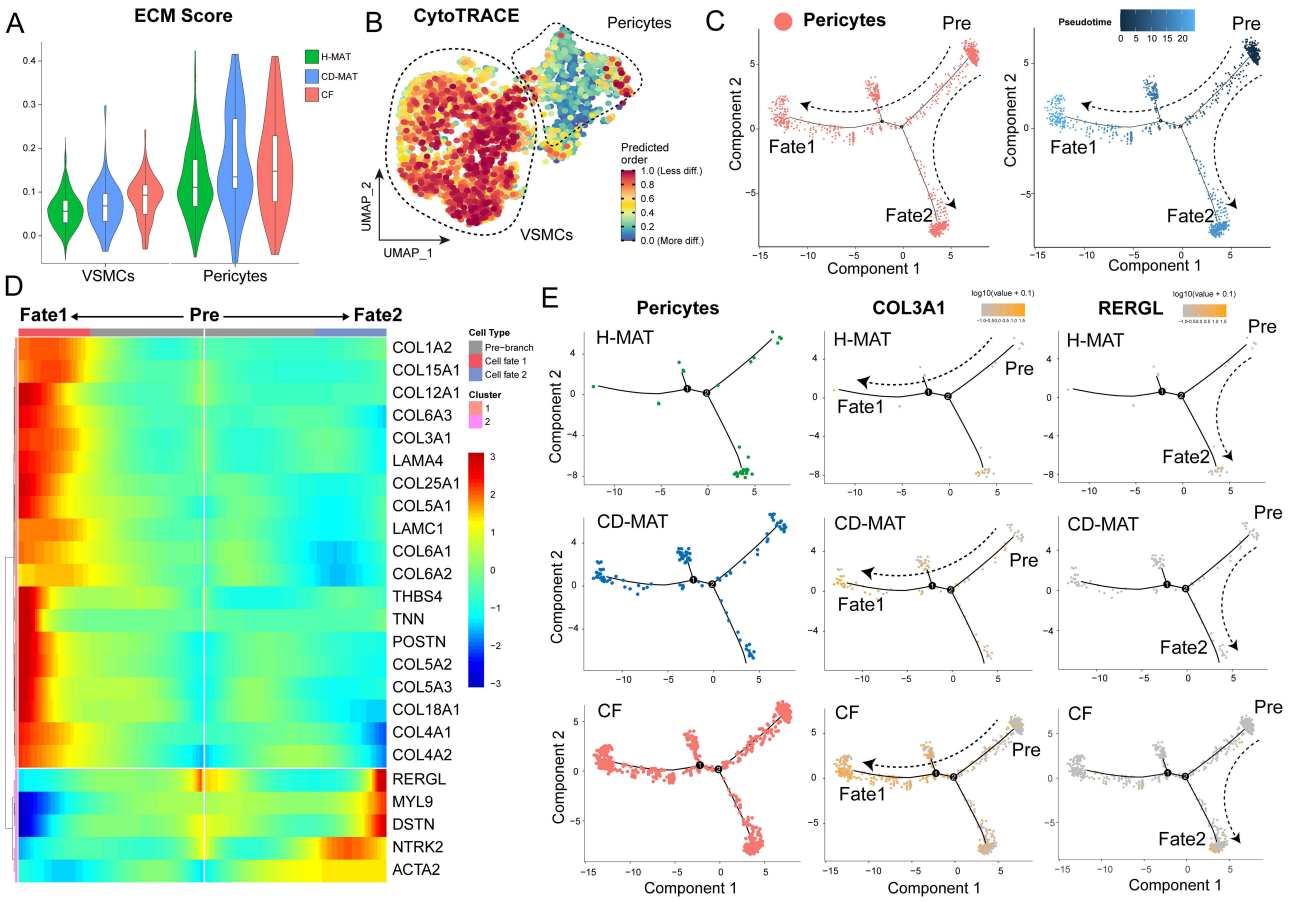

Figure 5 Pericytes in human MAT can transition into fibrotic and VSMC phenotypes. (**A**) Violin plot showing ECM score differences between VSMCs and pericytes. (**B**) UMAP plot of CytoTRACE analysis for VSMCs and pericytes (color intensity reflects differentiation potential; brighter = higher potential). (**C**) Monocle trajectory analysis of pericytes, identifying two distinct differentiation fates (Fate 1 and Fate 2) based on gene expression. Each point represents a single cell. (**D**) Heatmap showing expression patterns of ECM-related genes and VSMC-specific genes associated with the two pericyte fates (red = high expression, blue = low). (**E**) Pseudotime trajectory plots showing COL3A1 and RERGL expression levels across pericytes from different MAT groups. Color intensity reflects relative gene expression level.

Ex vivo Validation of Pericytes Transition to a Fibrotic Phenotype

We next examined the abundance of pericytes and VSMCs in the three groups of the primary scRNA-seq dataset. Both pericytes and VSMCs were significantly more numerous in CF than in H-MAT or CD-MAT (Figure 6A). We also performed immunofluorescence co-staining for STEAP4 (a pericyte marker) and COL3A1 on CD-MAT and CF tissue sections. CF tissue showed significantly more pericytes and greater collagen (COL3A1) deposition than CD-MAT (Figure 6B). Importantly, in both CD-MAT and CF, pericytes were observed along blood vessel walls with COL3A1 deposited around them (Figure 6B). This perivascular pattern was more pronounced in CF, which exhibited a marked increase in pericytes co-localized with COL3A1 (Figure 6B). These ex vivo observations are consistent with our pseudotime analysis.

In our scRNA-seq data, MCAM was expressed in both pericytes and VSMCs (with higher expression in VSMCs), whereas CD36 was expressed in pericytes but not in VSMCs (Figure 6C). Based on these markers, we isolated primary SVF cells from CD-MAT and used magnetic beads to sort $MCAM^{+}CD36^{+}$ cells, thereby enriching for pericytes (Figure 6D). Immunofluorescence confirmed that these $MCAM^{+}CD36^{+}$ cells expressed the pericyte marker STEAP4, as well as the mural cell markers MCAM and α-SMA (Figure 6D). To test their fibrogenic potential in vitro, we treated the $MCAM^{+}CD36^{+}$ cells with the pro-fibrotic factor TGF-β1 for 24 hours. This stimulation significantly upregulated core collagen-related genes (COL1A1, COL1A2, COL3A1) (Figure 6E) and markedly increased COL3A1 protein levels (Figure 6F). Collectively, these results indicate that pericytes can transition to a fibrotic phenotype in response to pro-fibrotic stimuli in vitro.

https://doi.org/10.2147/JIR.S528171

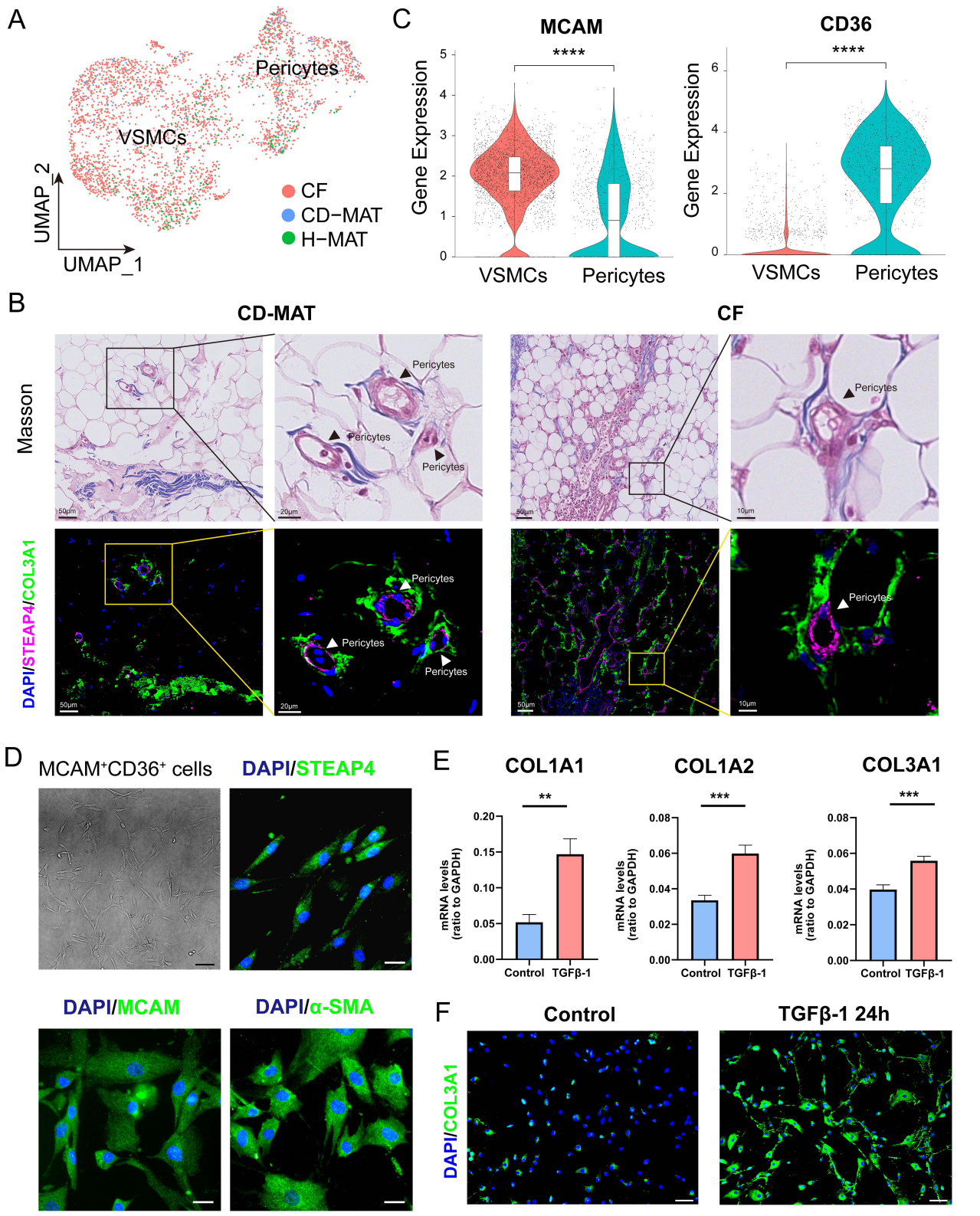

Figure 6 Pericytes are increased in CF and can adopt a fibrotic phenotype in vitro. (**A**) UMAP plot (scRNA-seq data) illustrating the distribution of VSMCs and pericytes in H-MAT, CD-MAT, and CF samples. (**B**) Representative Masson's trichrome staining and immunofluorescence co-staining images of CD-MAT and CF tissues, showing COL3A1 (green), STEAP4 (purple/magenta), and nuclei (DAPI, blue). (**C**) Violin plots comparing MCAM and CD36 expression in VSMCs vs pericytes. Statistical significance: ****$P < 0.0001$ (unpaired *t*-test). (**D**) Representative immunofluorescence images of isolated $MCAM^+CD36^+$ cells, confirming their expression of pericyte markers (STEAP4) and mural cell markers (MCAM, α-SMA). Scale bars: 20 μm. (**E**) Relative mRNA expression levels of COL1A1, COL1A2, and COL3A1 in cultured pericytes after 24-hour exposure to TGF-β1. Data are mean ± SD. Statistical significance: **$P < 0.01$; ***$P < 0.001$ (Mann–Whitney *U*-test). (**F**) Representative immunofluorescence staining showing increased COL3A1 expression in pericytes following 24-hour TGF-β1 stimulation. Scale bars: 100 μm.

Discussion

Increasing evidence has demonstrated a significant association between CF and CD disease activity, progression, and recurrence,[28,29] establishing CF as a potential therapeutic target.[30,31] The pathogenesis of CF involves adipocyte dysfunction, with fibrosis in CF tissue serving as an important contributing factor. Fibrosis is characterized by excessive ECM deposition, with stromal cells being the primary source of ECM components.[32,33] In this study, we identified varying degrees of tissue fibrosis in both CF and CD-MAT. Furthermore, we elucidated the cellular sources of excessive ECM production in these tissues, finding that MSCs and pericytes are the key SVF subpopulations responsible for MAT fibrosis. Notably, our findings highlight the capacity of pericytes to acquire a fibrogenic phenotype and synthesize substantial amounts of ECM, thereby contributing to MAT fibrosis.

While fibrosis in CF has been extensively characterized, the presence and extent of fibrosis in CD-MAT had remained unclear. CD-MAT, defined as MAT adjacent to intestinal segments without macroscopic inflammation in CD patients, has traditionally been regarded as relatively normal tissue.[6] By integrating previously reported scanning electron microscopy observations of MAT, newly generated histological data (H&E and Masson's trichrome staining), and reanalysis of the largest available paired transcriptomic dataset of CD patient MAT, we present the first evidence that CD-MAT exhibits moderate fibrosis compared to H-MAT. Prior analyses showed that CF contains fewer adipose-derived fibroblasts and a higher frequency of immune cells relative to H-MAT.[4] However, these differences diminish when comparing CF to CD-MAT, suggesting that CD-MAT may represent an intermediate state between healthy MAT and CF.[4] This notion is supported by our finding that both CVF and fibrosis-related gene expression levels in CD-MAT are intermediate between those in H-MAT and CF. Given that adipose tissue fibrosis is a hallmark of adipose tissue dysfunction and contributes to its functional impairment,[8,10] the presence of fibrosis in CD-MAT implies that MAT fibrosis might precede CF formation. Additionally, this finding indicates that CD-MAT likely exhibits some degree of adipose tissue dysfunction compared to H-MAT, with fibrosis potentially playing a significant role. These insights underscore the importance of focusing on both CF and CD-MAT in future investigations.

In the context of adipose tissue fibrosis, adipocyte progenitors expressing platelet-derived growth factor receptor-α (PDGFRα) have been identified as primary contributors to ECM production.[34] Compared to adipocytes, endothelial cells, or macrophages, PDGFRα^{+} cells express the highest levels of fibrotic markers in fibrotic adipose tissue. However, the main cellular drivers of MAT fibrosis had yet to be determined. Ha et al showed that human MAT adipocyte progenitors significantly upregulate ECM-related pathways.[4] Similarly, in our previous scRNA-seq study, we identified MSCs as adipocyte progenitors in MAT, marked by PDGFRα expression.[6] Notably, we identified a specialized subset of MSCs that accelerates CF formation.[6] In the current study, we likewise observed that MSCs in MAT are the SVF subpopulation with the highest fibrosis scores, far exceeding those of other stromal or immune cells. These findings implicate MSCs as the primary contributors to fibrosis in both CF and CD-MAT. However, we observed no significant differences in fibrosis scores among the three MSC subsets, suggesting that no single MSC subset disproportionately drives MAT fibrosis. In conclusion, although MSCs are clearly the principal SVF cell population responsible for MAT fibrosis, the specific mechanisms and drivers of this process remain to be elucidated in future studies.

Mural cells—the populations of cells surrounding blood vessels—include pericytes that wrap small-diameter vessels and VSMCs that encircle larger arteries and veins.[26] Research on vascular mural cells in human MAT is limited, primarily due to their significant heterogeneity across tissues and organs and the difficulty in distinguishing them from other stromal cells.[20,35,36] Single-cell RNA-seq of SVF cells has proven effective for identifying and distinguishing mural cell types. In previous MAT scRNA-seq studies, clusters expressing MCAM, NOTCH3, ACTA2 (α-SMA), and RGS5 were uniformly labeled as "pericytes".[4,6] However, by reanalyzing our single-cell dataset and validating with an independent dataset plus ex vivo immunofluorescence, we found that MCAM and ACTA2 are general markers for MAT mural cells rather than specific to pericytes. Furthermore, we determined that MAT mural cells can be subdivided into pericytes and VSMCs: pericytes express the specific marker STEAP4 and ECM-related genes, while VSMCs express the specific marker RERGL and smooth muscle genes.

In our study, both single-cell compositional analysis and in vitro immunostaining confirmed a marked increase in ECs and pericytes within CF, suggesting enhanced angiogenesis. A growing body of evidence supports a central role for

reciprocal signaling between ECs and pericytes in this process. In later stages of angiogenesis, tip ECs secrete platelet-derived growth factor-B (PDGF-B), which binds to PDGF receptor-β (PDGFRβ) on pericytes, promoting their recruitment and proliferation.[37,38] Direct EC–pericyte contact also activates transforming growth factor-β (TGF-β), which signals through activin receptor-like kinase 5 (ALK5) and downstream Smad2/3 in pericytes to promote their differentiation.[39] In addition, ECs regulate pericyte maturation via the Jagged1–Notch3 signaling axis.[40,41] In turn, pericyte–EC contact can stimulate EC proliferation by activating ALK1–Smad1/5 signaling, and can promote EC survival and vessel stabilization through pericyte secretion of vascular endothelial growth factor (VEGF), angiopoietin-1 (Ang1), and sphingosine-1-phosphate (S1P). Specifically, VEGF acts on VEGFR2, Ang1 activates the Tie2 receptor, and S1P signals through endothelial differentiation gene-1 (EDG-1, also known as S1PR1) on ECs.[42–44] Notably, recent studies suggest that pericytes may also contribute to the early stages of angiogenesis: pericyte expansion often precedes EC proliferation, and the absence or inhibition of pericyte activation impairs EC expansion.[45,46] Taken together, these findings indicate that enhanced angiogenesis in CF involves complex, bidirectional EC–pericyte communication, and that pericyte expansion is not merely a consequence but may actively drive pathological vascular remodeling. Future studies employing well-designed in vitro and in vivo models are warranted to dissect these dynamic interactions and clarify the mechanistic role of pericytes in CF-associated angiogenesis.

To our knowledge, this is the first study to demonstrate that pericytes in MAT can acquire a fibrotic phenotype, leading to tissue fibrosis. We observed that mural cells constitute another SVF subgroup with elevated ECM scores, among which pericytes exhibited higher ECM scores than VSMCs. Pericytes, as a key source of myofibroblasts, have garnered increasing attention for their pivotal role in fibrosis.[21,22,47] Specifically, renal NOTCH3^{+} RGS5^{+} PDGFRα^{-} pericytes, which serve as precursors to myofibroblasts, have been implicated in kidney fibrosis.[21] Similarly, cardiac pericytes in infarcted tissue show upregulation of fibrosis-associated genes, promoting ECM synthesis and tissue remodeling.[22] In our study, pericytes exhibited robust differentiation potential, accompanied by a significant increase in their population in CF. This expansion was associated with substantial collagen deposition in the perivascular regions surrounding these cells. Notably, pericytes in both CD-MAT and CF acquired a fibrotic phenotype, characterized by elevated expression of numerous core ECM genes, thereby contributing to fibrosis in these tissues. This finding further elucidates our earlier observation that a considerable portion of ECM in CD-MAT is prominently localized around blood vessels. Additionally, we identified a unique differentiation trajectory of pericytes: they differentiated into VSMCs in H-MAT and CF, concomitant with upregulation of their marker gene RERGL and other smooth muscle–associated genes. These findings suggest that pericytes may serve as a precursor cell population for VSMCs, potentially playing a critical role in early vascular development. However, this hypothesis requires further experimental validation to establish the precise mechanisms and functional significance of this differentiation pathway.

Despite identifying MSCs and pericytes as key contributors to fibrosis in CD-MAT and CF, the upstream signals that trigger their activation and ECM production remain incompletely understood and require further investigation. Notably, our study lacks in vivo functional validation to directly confirm the fibrogenic role of pericytes. While our conclusions are supported by transcriptomic reanalysis, in vitro experiments, and immunostaining of human samples, future studies employing lineage-tracing models or conditional pericyte manipulation in animals will be essential to causally establish their contribution to MAT fibrosis. In addition, the potential links between MAT fibrosis, adipose tissue dysfunction, and intestinal stricture formation remain to be fully elucidated.

Conclusion

In summary, our study demonstrates that both CF and CD-MAT tissues exhibit fibrosis to varying degrees in the context of CD. Both CF and CD-MAT show significant perivascular ECM deposition, with CF showing a particularly marked increase in vascularity and pericyte abundance. We establish a critical link between angiogenesis and MAT fibrosis, identifying pericytes as a pivotal subpopulation mediating this connection. Specifically, our findings reveal that pericytes in both CF and CD-MAT acquire a fibrotic phenotype, which drives excessive ECM accumulation and promotes fibrosis progression.

Data Sharing Statement

The datasets used in this study are publicly available via the GEO database (http://www.ncbi.nlm.nih.gov/geo). Further details can be obtained from the corresponding author.

Ethical Approval and Consent to Participate

Patients were enrolled at Nanfang Hospital (Guangzhou, China) in compliance with the Declaration of Helsinki. Ethical approval was obtained from the Medical Ethics Committee of Nanfang Hospital of Southern Medical University (approval number: NFEC-2024-495). Written informed consent was obtained from all participants prior to the collection of specimens and clinical data.

Acknowledgments

The authors thank the contributors of GEO datasets GSE227376, GSE215001, and GSE156776 for making their data available.

Author Contributions

All authors made a significant contribution to the work reported, whether that is in the conception, study design, execution, acquisition of data, analysis and interpretation, or in all these areas; took part in drafting, revising or critically reviewing the article; gave final approval of the version to be published; have agreed on the journal to which the article has been submitted; and agree to be accountable for all aspects of the work.

Funding

This research was supported by the National Natural Science Foundation of China (grant nos. 82070534, 82470539), the Natural Science Foundation of Guangdong Province (grant nos. 2023A1515010729, 2023A1515012537), and the Guangdong Basic and Applied Basic Research Fund (grant no. 2023A1515140170).

Disclosure

The authors report no conflicts of interest in this work.

References

1. Torres J, Mehandru S, Colombel J-F, Peyrin-Biroulet L. Crohn's disease. *Lancet*. 2017;389(10080):1741–1755. doi:10.1016/s0140-6736(16)31711-1
2. Feuerstein JD, Cheifetz AS. Crohn disease: epidemiology, diagnosis, and management. *Mayo Clin Proc*. 2017;92(7):1088–1103. doi:10.1016/j.mayocp.2017.04.010
3. Rieder F, Fiocchi C, Rogler G. Management, and treatment of fibrosis in patients with inflammatory bowel diseases. *Gastroenterology*. 2017;152(2):340–350.e6. doi:10.1053/j.gastro.2016.09.047
4. Ha CWY, Martin A, Sepich-Poore GD, et al. Translocation of viable gut microbiota to mesenteric adipose drives formation of creeping fat in humans. *Cell*. 2020;183(3):666–683.e17. doi:10.1016/j.cell.2020.09.009
5. Atreya R, Siegmund B. Location is important: differentiation between ileal and colonic crohn's disease. *Nat Rev Gastroenterol Hepatol*. 2021;18(8):544–558. doi:10.1038/s41575-021-00424-6
6. Wu F, Wu F, Zhou Q, et al. A $CCL2^{+}DPP4^{+}$ subset of mesenchymal stem cells expedites aberrant formation of creeping fat in humans. *Nat Commun*. 2023;14(1):5830. doi:10.1038/s41467-023-41418-z
7. Xiong S, Whitehurst CE, Li L, et al. Reverse translation approach generates a signature of penetrating fibrosis in crohn's disease that is associated with anti-TNF response. *Gut*. 2022;71(7):1289–1301. doi:10.1136/gutjnl-2020-323405
8. Zuo L, Li J, Zhang X, et al. Aberrant mesenteric adipose extracellular matrix remodelling is involved in adipocyte dysfunction in Crohn's disease: the role of TLR-4-mediated macrophages. *J Crohns Colitis*. 2022;16(11):1762–1776. doi:10.1093/ecco-jcc/jjac087
9. Xiong S, Tan J, Wang Y, et al. Fibrosis in fat: from other diseases to Crohn's disease. *Front Immunol*. 2022;13:935275. doi:10.3389/fimmu.2022.935275
10. Crewe C, An YA, Scherer PE. The ominous triad of adipose tissue dysfunction: inflammation, fibrosis, and impaired angiogenesis. *J Clin Invest*. 2017;127(1):74–82. doi:10.1172/jci88883
11. Henegar C, Tordjman J, Achard V, et al. Adipose tissue transcriptomic signature highlights the pathological relevance of extracellular matrix in human obesity. *Genome Biol*. 2008;9(1):R14. doi:10.1186/gb-2008-9-1-r14
12. Seo BR, Bhardwaj P, Choi S, et al. Obesity-dependent changes in interstitial ECM mechanics promote breast tumorigenesis. *Sci Transl Med*. 2015;7(301):301ra130. doi:10.1126/scitranslmed.3010467

13. Abe I, Teshima Y, Kondo H, et al. Association of fibrotic remodeling and cytokines/chemokines content in epicardial adipose tissue with atrial myocardial fibrosis in patients with atrial fibrillation. *Heart Rhythm*. 2018;15(11):1717–1727. doi:10.1016/j.hrthm.2018.06.025
14. Barboza E, Hudson J, Chang WP, et al. Profibrotic infrapatellar fat pad remodeling without m1 macrophage polarization precedes knee osteoarthritis in mice with diet-induced obesity. *Arthritis Rheumatol*. 2017;69(6):1221–1232. doi:10.1002/art.40056
15. Theocharis AD, Skandalis SS, Gialeli C, Karamanos NK. Extracellular matrix structure. *Adv Drug Deliv Rev*. 2016;97:4–27. doi:10.1016/j.addr.2015.11.001
16. Bastard JP, Maachi M, Lagathu C, et al. Recent advances in the relationship between obesity, inflammation, and insulin resistance. *Eur Cytokine Netw*. 2006;17(1):4–12.
17. Bilson J, Oquendo CJ, Read J, et al. Markers of adipose tissue fibrogenesis associate with clinically significant liver fibrosis and are unchanged by synbiotic treatment in patients with NAFLD. *Metabolism*. 2024;151:155759. doi:10.1016/j.metabol.2023.155759
18. Anthony Sarah R, Guarnieri Adrienne R, Gozdiff A, Helsley Robert N, Phillip Owens A, Tranter M. Mechanisms linking adipose tissue inflammation to cardiac hypertrophy and fibrosis. *Clin Sci*. 2019;133(22):2329–2344. doi:10.1042/cs20190578
19. Martin JC, Chang C, Boschetti G, et al. Single-Cell analysis of Crohn's disease lesions identifies a pathogenic cellular module associated with resistance to anti-TNF therapy. *Cell*. 2019;178(6):1493–1508.e20. doi:10.1016/j.cell.2019.08.008
20. Baek S-H, Maiorino E, Kim H, Glass K, Raby BA, Yuan K. Single cell transcriptomic analysis reveals organ specific pericyte markers and identities. *Front Cardiovasc Med*. 2022;9:876591. doi:10.3389/fcvm.2022.876591
21. Kuppe C, Ibrahim MM, Kranz J, et al. Decoding myofibroblast origins in human kidney fibrosis. *Nature*. 2020;589(7841):281–286. doi:10.1038/s41586-020-2941-1
22. Alex L, Tuleta I, Hernandez SC, et al. Cardiac pericytes acquire a fibrogenic phenotype and contribute to vascular maturation after myocardial infarction. *Circulation*. 2023;148(11):882–898. doi:10.1161/circulationaha.123.064155
23. Naba A, Clauser KR, Ding H, Whittaker CA, Carr SA, Hynes RO. The extracellular matrix: tools and insights for the "omics" era. *Matrix Biol*. 2016;49:10–24. doi:10.1016/j.matbio.2015.06.003
24. Kim K, Park S, Lee Y, et al. Transcriptomic profiling and cellular composition of creeping fat in Crohn's disease. *J Crohns Colitis*. 2024;18(2):223–232. doi:10.1093/ecco-jcc/jjad141
25. Siekmann AF. Biology of vascular mural cells. *Development*. 2023;150(16):dev200271. doi:10.1242/dev.200271
26. van Splunder H, Villacampa P, Martínez-Romero A, Graupera M. Pericytes in the disease spotlight. *Trends Cell Biol*. 2024;34(1):58–71. doi:10.1016/j.tcb.2023.06.001
27. Gulati GS, Sikandar SS, Wesche DJ, et al. Single-cell transcriptional diversity is a hallmark of developmental potential. *Science*. 2020;367(6476):405–411. doi:10.1126/science.aax0249
28. Mao R, Kurada S, Gordon IO, et al. The mesenteric fat and intestinal muscle interface: creeping fat influencing stricture formation in Crohn's disease. *Inflamm Bowel Dis*. 2019;25(3):421–426. doi:10.1093/ibd/izy331
29. Li Y, Zhu W, Zuo L, Shen B. The role of the mesentery in crohn's disease: the contributions of nerves, vessels, lymphatics, and fat to the pathogenesis and disease course. *Inflamm Bowel Dis*. 2016;22(6):1483–1495. doi:10.1097/mib.0000000000000791
30. Zuo L, Ge S, Ge Y, et al. The adipokine metrnl ameliorates chronic colitis in Il-10$^{-/-}$ mice by attenuating mesenteric adipose tissue lesions during spontaneous colitis. *J Crohns Colitis*. 2019;13(7):931–941. doi:10.1093/ecco-jcc/jjz001
31. Li Y, Zuo L, Zhu W, et al. Telmisartan attenuates the inflamed mesenteric adipose tissue in spontaneous colitis by mechanisms involving regulation of neurotensin/microRNA-155 pathway. *Biochem Pharmacol*. 2015;93(4):461–469. doi:10.1016/j.bcp.2014.12.020
32. Henderson NC, Rieder F, Wynn TA. Fibrosis: from mechanisms to medicines. *Nature*. 2020;587(7835):555–566. doi:10.1038/s41586-020-2938-9
33. Talbott HE, Mascharak S, Griffin M, Wan DC, Longaker MT. Wound healing, fibroblast heterogeneity, and fibrosis. *Cell Stem Cell*. 2022;29(8):1161–1180. doi:10.1016/j.stem.2022.07.006
34. Marcelin G, Ferreira A, Liu Y, et al. A PDGFRα-mediated switch toward CD9^{high} adipocyte progenitors controls obesity-induced adipose tissue fibrosis. *Cell Metab*. 2017;25(3):673–685. doi:10.1016/j.cmet.2017.01.010
35. Crisan M, Yap S, Casteilla L, et al. A perivascular origin for mesenchymal stem cells in multiple human organs. *Cell Stem Cell*. 2008;3(3):301–313. doi:10.1016/j.stem.2008.07.003
36. Rieder F, Mukherjee PK, Massey WJ, Wang Y, Fiocchi C. Fibrosis in IBD: from pathogenesis to therapeutic targets. *Gut*. 2024;73(5):854–866. doi:10.1136/gutjnl-2023-329963
37. Hoch RV, Soriano P. Roles of PDGF in animal development. *Development*. 2003;130(20):4769–4784. doi:10.1242/dev.00721
38. Betsholtz C. Insight into the physiological functions of PDGF through genetic studies in mice. *Cytokine Growth Factor Rev*. 2004;15(4):215–228. doi:10.1016/j.cytogfr.2004.03.005
39. Goumans M-J, Valdimarsdottir G, Itoh S, Rosendahl A, Sideras P, ten Dijke P. Balancing the activation state of the endothelium via two distinct TGF-beta type I receptors. *EMBO J*. 2002;21(7):1743–1753. doi:10.1093/emboj/21.7.1743
40. Machuca-Parra AI, Bigger-Allen AA, Sanchez AV, et al. Therapeutic antibody targeting of Notch3 signaling prevents mural cell loss in CADASIL. *J Exp Med*. 2017;214(8):2271–2282. doi:10.1084/jem.20161715
41. Diéguez-Hurtado R, Kato K, Giaimo BD, et al. Loss of the transcription factor RBPJ induces disease-promoting properties in brain pericytes. *Nat Commun*. 2019;10(1):2817. doi:10.1038/s41467-019-10643-w
42. Darland DC, Massingham LJ, Smith SR, Piek E, Saint-Geniez M, D'Amore PA. Pericyte production of cell-associated VEGF is differentiation-dependent and is associated with endothelial survival. *Dev Biol*. 2003;264(1):275–288. doi:10.1016/S0012-1606(03)00492-5
43. Teichert M, Milde L, Holm A, et al. Pericyte-expressed Tie2 controls angiogenesis and vessel maturation. *Nat Commun*. 2017;8:16106. doi:10.1038/ncomms16106
44. Gaengel K, Niaudet C, Hagikura K, et al. The sphingosine-1-phosphate receptor S1PR1 restricts sprouting angiogenesis by regulating the interplay between VE-cadherin and VEGFR2. *Dev Cell*. 2012;23(3):587–599. doi:10.1016/j.devcel.2012.08.005
45. Figueiredo AM, Villacampa P, Diéguez-Hurtado R, et al. Phosphoinositide 3-kinase-regulated pericyte maturation governs vascular remodeling. *Circulation*. 2020;142(7):688–704. doi:10.1161/circulationaha.119.042354
46. Mäe MA, He L, Nordling S, et al. Single-cell analysis of blood-brain barrier response to pericyte loss. *Circ Res*. 2021;128(4):e46–e62. doi:10.1161/circresaha.120.317473

47. Dias DO, Kim H, Holl D, et al. Reducing pericyte-derived scarring promotes recovery after spinal cord injury. *Cell*. 2018;173(1):153–165.e22. doi:10.1016/j.cell.2018.02.004